# Scaling purely elastic instability of strongly shear thinning polymer solutions

Pegah Shakeri ◉,*,† Michael Jung ◉,*,‡ and Ralf Seemann ◉

*Experimental Physics, Saarland University, 66123 Saarbrücken, Germany*
*and Max Planck Institute for Dynamics and Self-Organization, 37077 Göttingen, Germany*

Flow of viscoelastic polymer solutions in curved channels exhibits instability caused by the elastic nature of polymers even at low Reynolds numbers. However, scaling of the onset of this purely elastic instability in semidilute polymer solutions has not been previously reported. Here we experimentally investigate the flow of highly elastic polymer solutions above their overlap concentrations using pressure measurements and particle image velocimetry. We demonstrate that the onset of instability can be scaled by including shear dependent rheological properties of the polymer solutions in the nonlinear stability analysis. As a result, a universal criterion as function of normalized polymer concentration is provided for scaling the onset of purely elastic instability in the semidilute regime regardless of the type and molecular weight of the polymer.

Purely elastic instability is a well-known phenomenon occurring during the flow of viscoelastic polymer solutions and melts at vanishing Reynolds numbers Re. This instability can be attributed to nonlinear elastic stresses, arising from the stretching and relaxing of flexible polymers, which do not fully dissipate beyond a critical shear rate [1–6]. The occurrence of purely elastic instability can be beneficial for practical applications such as microfluidic mixing, heat transfer, and mobilization of capillary entrapments [7–9]. However, in multiple processes in food and cosmetics industry [10,11], as well as polymer extrusion [12], the occurrence of purely elastic instability is undesirable. Therefore, it is crucial to estimate the conditions under which the purely elastic instability occurs, in terms of the rheology of the fluid and the geometrical properties of the flow.

Polymers are inherently nonuniformly stretched during flow, resulting in an anisotropic distribution of three-dimensional stresses. The difference between the stress component in the flow direction and the stress component in the transverse direction is called the first normal stress difference $N_1$. In curved geometries when $N_1$ becomes substantially larger than the shear stress $\tau$, elastic stresses dominate, and polymers are pulled toward regions with higher streamline curvature [4,9]. As a result, the laminar flow paths are disturbed and the polymers are spatially and temporally subjected to different shear rates. Consequently, the polymers

repeatedly store and release elastic stresses during flow, which leads to the emergence of an unstable flow above a certain threshold. Pakdel and McKinley observed that in a curved geometry the onset of this instability can be scaled with respect to the ratio of the first normal stress difference $N_1$ to the shear stress $\tau$ and the curvature of the streamline [13,14]. Thus, the criteria for scaling the onset of pure elastic instability can be formulated as in Eq. (1) [4]:

$$\sqrt{\frac{l}{\mathcal{R}} \frac{|N_1|}{|\tau|}} \geqslant M_{\mathrm{crit}}, \tag{1}$$

where $l$ is a characteristic length scale and $\mathcal{R}$ is the radius of streamline curvature. Since, for a given geometry, the onset of instability is governed merely by the stress ratio, $M_{\mathrm{crit}}$ can be considered as a critical stress factor. However, it is essential to notice that this approach does not provide a universal numerical value for $M_{\mathrm{crit}}$, but rather describes how the onset of nonlinearity scales with respect to the rheological and geometrical properties [15]. The value of $M_{\mathrm{crit}}$ depends on the type and concentration of the polymer and salt in the solution, as well as on the type of solvent, and is commonly in the range of 1 to 6 [4,16].

This scaling is often used for polymer solutions in the dilute regime, i.e., for polymer concentrations below the overlap concentration $c^*$, in which the viscosity $\eta$, and the relaxation time $\lambda$ can be assumed to be independent on the shear rate $\dot{\gamma}$. Here, the ratio of $|N_1|$ to $|\tau|$ is linearly dependent on the shear rate, and the characteristic length can be estimated by $l = U \lambda_0$, where $U$ is the average flow velocity and $\lambda_0$ is the longest polymer relaxation time [4,16–20]. However, above the overlap concentration $c^*$ the polymer behavior during flow is more complicated. Both $\eta(\dot{\gamma})$ and $\lambda(\dot{\gamma})$ show significant nonlinear dependency on the shear rate [21,22]. Using the longest polymer relaxation time $\lambda_0$ to estimate the characteristic length, as commonly done in literature [23–25], leads to unrealistically large timescales which do not represent the

---

*These authors contributed equally to this work.

†pegah.shakeri@physik.uni-saarland.de

‡michael.jung@physik.uni-saarland.de

actual dynamics of the polymers in flow in this concentration regime [25]. Moreover, unlike the dilute regime, the ratio of the first normal stress difference to the shear stress in Eq. (1) is not linearly dependent on the shear rate due to the nonquadratic dependence of $N_1$ on the shear rate, and the nonlinear dependence of $|\tau|$ on the shear rate. Therefore, the assumption of a constant relaxation time is not reasonable, and it is necessary to adopt a realistic approach for scaling the onset of purely elastic instability in the semidilute regime that faithfully reflects the rheological properties of the polymers.

In this paper, we present a practical scaling of the onset of purely elastic instability for strongly shear thinning, highly elastic polymer solutions in the semidilute regime. To this aim, we determine the onset of purely elastic instability of various polymer solutions in a microfluidic serpentine channel via pressure measurements and particle image velocimetry ($\mu$PIV). We scale the onset of the observed instability in our experiments by considering the White-Metzner fluid model to account for the shear dependence of the rheological properties of the polymer solutions. Applying this scaling, the onset of purely elastic instability as function of normalized polymer concentration collapses into a universal master curve independent of polymer type and molecular weight, confirming the suggested approach.

The microfluidic channel used in our experiments is fabricated from UV-curable glue NOA 83H (Norland optical adhesives) by soft lithography using standard protocols [9,26]. The microfluidic serpentine channel consisting of 33 consecutive half-loops has the total length of $l \approx 26$ mm, width of $w \approx 0.125$ mm, height of $h \approx 0.036$ mm, and an inner bend radius of curvature of $r_i \approx 0.125$ mm. The inlet of the microfluidic channel is connected to a high-precision, pulsation-free syringe pump (neMESYS, Cetoni GmbH) that enables fluid injection at a controlled volumetric flow rate. The outlet is connected to a liquid reservoir at the same height as the microfluidic device to avoid additional hydrostatic pressure difference. The hydrodynamic pressure drop $\Delta P$ inside the serpentine channel is measured by a differential pressure sensor (26PC series, Honeywell) mounted between inlet and outlet. A sketch of the microfluidic channel is provided in the inset of Fig. 1(a).

To represent a wide range of common polymer types that are prone to purely elastic instability, we use two commercial polyelectrolytes, the partially hydrolyzed polyacrylamides (HPAM, 30% hydrolysis) Flopaam 3630 ($M_{w,3630} \approx$ 18.7 MDa) and Flopaam 3330 ($M_{w,3330} \approx 6.5$ MDa) dissolved in 17 mM NaCl solution as well as polyethylene oxide (PEO, $M_{w,\text{PEO}} \approx 8.0$ MDa) dissolved in ultrapure water. The sample solutions with different concentrations are prepared following standard protocols [9]. It should be mentioned that the salt concentration in case of the HPAM solutions is rather in the low-salt limit and not sufficient to screen all charges of the polyelectrolyte [27]. The densities of all utilized solutions were determined to $\varrho = (1.00 \pm 0.01)$ g/cm$^3$ by a pycnometer. A full rheological characterization including steady shear step measurements to determine $\eta(\dot{\gamma})$ and $N_1(\dot{\gamma})$ as well as small amplitude frequency sweep tests to determine the storage modulus $G'(\omega)$ and the loss modulus $G''(\omega)$ are performed using a rotational rheometer (HAAKE MARS 40, Thermo Scientific). The data are presented in the
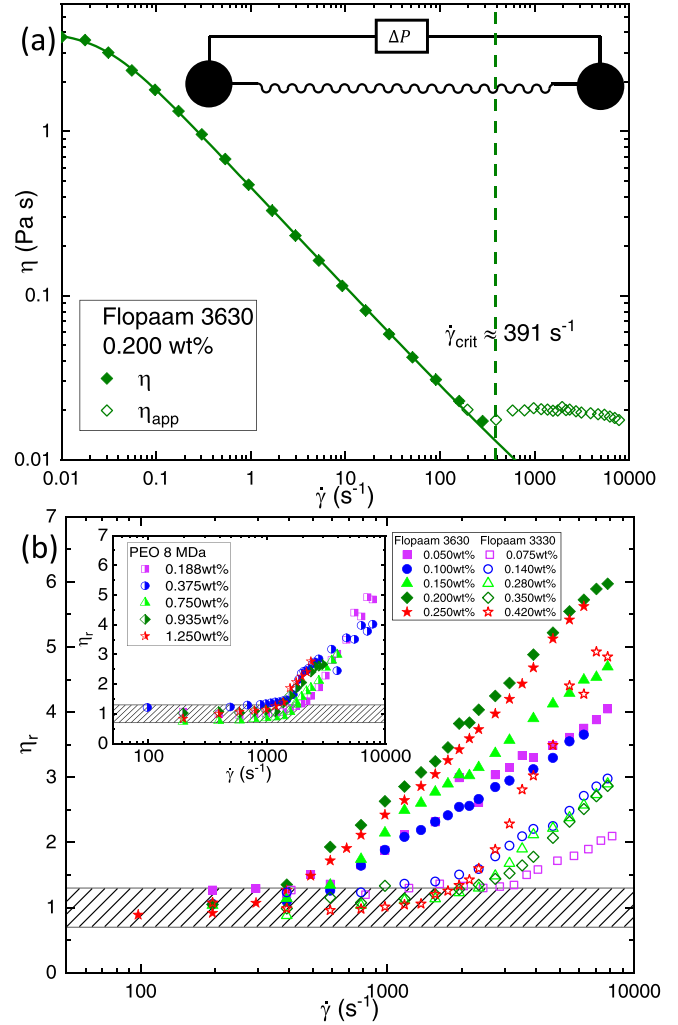


FIG. 1. (a) The shear viscosity $\eta(\dot{\gamma})$ measured using a rheometer (filled symbols) and apparent viscosity $\eta_{\text{app}}(\dot{\gamma})$ (open symbols) calculated from the pressure difference $\Delta P$ along the serpentine channel (sketch in the inset) for 0.200 wt% Flopaam 3630. The line is a fit to the Carreau-Yasuda model [Eq. (3)]. The dashed vertical line indicates the critical shear rates $\dot{\gamma}_{\text{crit}}$. (b) Reduced viscosity $\eta_r(\dot{\gamma}) = \eta_{\text{app}}(\dot{\gamma})/\eta(\dot{\gamma})$ as function of the shear rate $\dot{\gamma}$ for Flopaam 3630 and 3330. The inset shows the respective data for PEO 8MDa. The shaded area indicates the initial plateau within the experimental accuracy.

Supplemental Material (SM) [28]. The critical overlap concentrations $c^*$ of the respective polymer types was determined using the Huggins-Kraemer method [29] to be $c^*_{3630} \approx$ 0.0082 wt%, $c^*_{3330} \approx 0.0137$ wt%, and $c^*_{\text{PEO}} \approx 0.0375$ wt% in agreement with literature values [9,30,31]. To be safely in the semidilute regime for each polymer type, the concentrations are chosen to cover the range from $5 \times c^*$ to $30 \times c^*$. Comparison of the power-law exponents of the respective zero shear viscosity (data in SM [28]) as function of concentration with literature values [25,27,30,32] confirms that the polymer chains remain unentangled below $10 \times c^*$ and become entangled at higher polymer concentrations.

TABLE I. Overview of the critical shear rate $\dot{\gamma}_{\mathrm{crit}}$, and $M_{\mathrm{crit}}$ at the onset of purely elastic instability for the utilized polymer solutions.

| Flopaam 3630 | $c/c^*$ | $\dot{\gamma}_c$ [s$^{-1}$] | $M_c$ | Flopaam 3330 | $c/c^*$ | $\dot{\gamma}_c$ [s$^{-1}$] | $M_c$ | PEO 8 MDa | $c/c^*$ | $\dot{\gamma}_c$[s$^{-1}$] | $M_c$ |
|---|---|---|---|---|---|---|---|---|---|---|---|
| 0.050 wt% | 6 | 783 ± 39 | 9.9 ± 0.6 | 0.075 wt% | 5 | 3100 ± 39 | 12.9 ± 0.8 | 0.188 wt% | 5 | 1566 ± 39 | 18.3 ± 1.2 |
| 0.100 wt% | 12 | 587 ± 39 | 7.5 ± 0.5 | 0.140 wt% | 10 | 2741 ± 39 | 10.6 ± 0.7 | 0.375 wt% | 10 | 1468 ± 39 | 6.3 ± 0.4 |
| 0.150 wt% | 18 | 587 ± 39 | 6.9 ± 0.5 | 0.280 wt% | 20 | 2741 ± 39 | 5.1 ± 0.3 | 0.750 wt% | 20 | 1417 ± 39 | 4.8 ± 0.3 |
| 0.200 wt% | 24 | 391 ± 39 | 3.7 ± 0.2 | 0.350 wt% | 25 | 2349 ± 39 | 4.3 ± 0.3 | 0.938 wt% | 25 | 1370 ± 39 | 4.5 ± 0.3 |
| 0.250 wt% | 30 | 391 ± 39 | 4.3 ± 0.3 | 0.420 wt% | 30 | 1566 ± 39 | 3.5 ± 0.2 | 1.250 wt% | 30 | 1175 ± 39 | 3.6 ± 0.2 |

In our microfluidic experiment, we stepwise increase the flow rate and measure the corresponding pressure drop $\Delta P$ across the serpentine channel. This pressure drop can be converted to an apparent viscosity $\eta_{\mathrm{app}}(\dot{\gamma}) = \tau(\dot{\gamma})/\dot{\gamma}$, where the shear stress in a serpentine channel is approximated by $\tau = (\Delta P\, H\, W)/[2L(W + H)]$ [33], while the shear rate is approximated by $\dot{\gamma} = 4Q/(\pi\, r^3)$ with the equivalent radius of $r = \sqrt{(W\,H)/\pi}$ [34]. It should be noted that this approximation of apparent shear rate $\dot{\gamma}$ is commonly recommended for aspect ratios $H/W \approx 1$. For smaller aspect ratios, Hartnett and Kostic [35] proposed a correction that also includes the Rabinowitch relation [36] to account for the shear thinning of polymer solution and nonparabolic velocity profile. However, we have confirmed that for the aspect ratio $H/W \approx 0.3$ used in this work, the apparent viscosity $\eta_{\mathrm{app}}(\dot{\gamma})$ exhibits a good agreement with the bulk viscosity values (see the Supplemental Material [28]). Thus, the given approximation is reliable, and the corrections are not essential. Furthermore, it is important to note that we employ a "point-wise" method and assume that for a particular flow rate the corresponding apparent shear rate, viscosity, and relaxation time can be described by constant values.

Comparison of the apparent viscosity $\eta_{\mathrm{app}}(\dot{\gamma})$ with the extrapolated bulk viscosity values $\eta(\dot{\gamma})$ in Fig. 1(a) reveals that above a critical shear rate, $\eta_{\mathrm{app}}(\dot{\gamma})$ deviates from $\eta(\dot{\gamma})$. Figure 1(b) shows the reduced viscosity $\eta_r(\dot{\gamma}) = \eta_{\mathrm{app}}(\dot{\gamma})/\eta(\dot{\gamma})$ as function of the shear rate $\dot{\gamma}$ for all studied polymer solutions. We identify the critical shear rate $\dot{\gamma}_{\mathrm{crit}}$, listed in Table I, at the onset of instability when the reduced viscosity exceeds 1.15. For a given polymer type, $\dot{\gamma}_{\mathrm{crit}}$ decreases only slightly with increasing concentration. These observations are in agreement with those of Howe et al. [30] who have reported that $\dot{\gamma}_{\mathrm{crit}}$ is independent of polymer concentration above $c \approx 10 \times c^*$ and is inversely proportional to $M_w^2$.

The serpentine geometry with rectangular cross section requires the consideration of two Reynolds numbers to ensure that inertial forces are negligible throughout the geometry. For channel flows, the Reynolds number is usually defined as $\mathrm{Re}_c = \varrho\, U\, r/\eta$ with the equivalent radius $r$ as the characteristic length, whereas the average velocity is approximated by $U = Q/(W\,H)$. To account for centrifugal inertia in curvilinear flow, the radius of curvature of the serpentine channel $r_i$ is used as the characteristic length and thus $\mathrm{Re}_s = \varrho\, U\, r_i/\eta$. The maximum Reynolds numbers of our presented experiments are $\mathrm{Re}_c \approx 1$ and $\mathrm{Re}_s \approx 4$. Therefore, we can conclude that the contribution of inertia to the flow is negligible. To verify the purely elastic origin of the observed instability, we perform $\mu$PIV (LaVison) measurements by adding 0.05 wt% 1-$\mu$m red fluorescent particles (FluoroMax, Thermo Fisher) to the polymer solution. The particles are excited with a laser

wavelength of 532 nm. Double-frame images with short time differences (0.1 ms < $dt$ < 0.8 ms), depending on the flow velocity, are recorded from the light emitted by the particles. Cross correlating these double frames, we obtain the velocity field in the serpentine channel. Figure 2(a) demonstrates the velocity fields at the middle half-bend of the serpentine channel averaged over 50 s for two different shear rates. Below the onset of purely elastic instability (left side), a laminar flow is observed whereas above the onset of purely elastic instability the velocity field (right side) deviates from a laminar flow. In the latter stage, unlike the laminar velocity profile, the maximum velocity is shifted toward the outer bend, i.e., toward the larger radius of curvature. The power spectra density of the local velocity fluctuations at the center of the middle half-bend of the serpentine channel [indicated by a (+) sign in Fig. 2(a)] are shown for four shear rates below and above the onset of flow instability in Figs. 2(b)–2(e) (further details in the Supplemental Material [28]). Indeed, the power-law decay $\sim f^{-\beta}$ with a characteristic exponent $\beta \approx 2$, in the range of 1 to 10 Hz at sufficiently high flow rates, is larger than the Kolmogorov scale of 5/3 associated with the inertial turbulence, suggesting that the mechanism of turbulence is not associated with inertia [37]. Similar exponents of $\beta$ in the range of 2 to 3 have been reported in the literature for semidilute polymer solutions at highly elastic turbulent stage [23,38,39].

In order to scale the onset of the instability observed in our experiments, we require both a rheological description of the fluids as well as geometrical properties of the flow channel, as suggested by Eq. (1). The polymer solutions used in our experiments exhibit strongly shear-dependent viscosity as well as a nonquadratic first normal stress difference (data in the Supplemental Material [28]). The behavior of such polymer solutions is described based on the White-Metzner constitutive fluid model [9,19,25,40]. The basic concept of this model is to define a total stress tensor $\boldsymbol{\tau} = \boldsymbol{\tau_1} + \boldsymbol{\tau_2}$, and a total viscosity $\eta = \eta_1 + \eta_2$ that are related by the deformation rate tensor $\mathbf{D}$ [21,41,42]. The pure viscous component of the stress tensor $\boldsymbol{\tau_2}$ is defined as $\boldsymbol{\tau_2} = 2\,\eta_2\,\mathbf{D}$, where $\eta_2$ is the solvent viscosity. $\boldsymbol{\tau_1}$ is defined by

$$\boldsymbol{\tau_1} + [\eta(\dot{\gamma})/G_0]\overset{\triangledown}{\boldsymbol{\tau_1}} = 2\,\eta_1(\dot{\gamma})\,\mathbf{D}, \tag{2}$$

where $\overset{\triangledown}{\boldsymbol{\tau_1}}$ is the upper convected time derivative. The shear rate is defined as $\dot{\gamma} = \sqrt{2\,tr(\mathbf{D}^2)}$ and the total shear stress is given by $\tau = 2\,\eta(\dot{\gamma})\,\dot{\gamma}$. The shear-dependent total viscosity of the polymer solution $\eta(\dot{\gamma})$ is described by the Carreau-Yasuda model [21,22]:

$$\eta(\dot{\gamma}) - \eta_{\infty} = (\eta_0 - \eta_{\infty})[1 + (\Lambda\dot{\gamma})^a]^{\frac{n-1}{a}}. \tag{3}$$
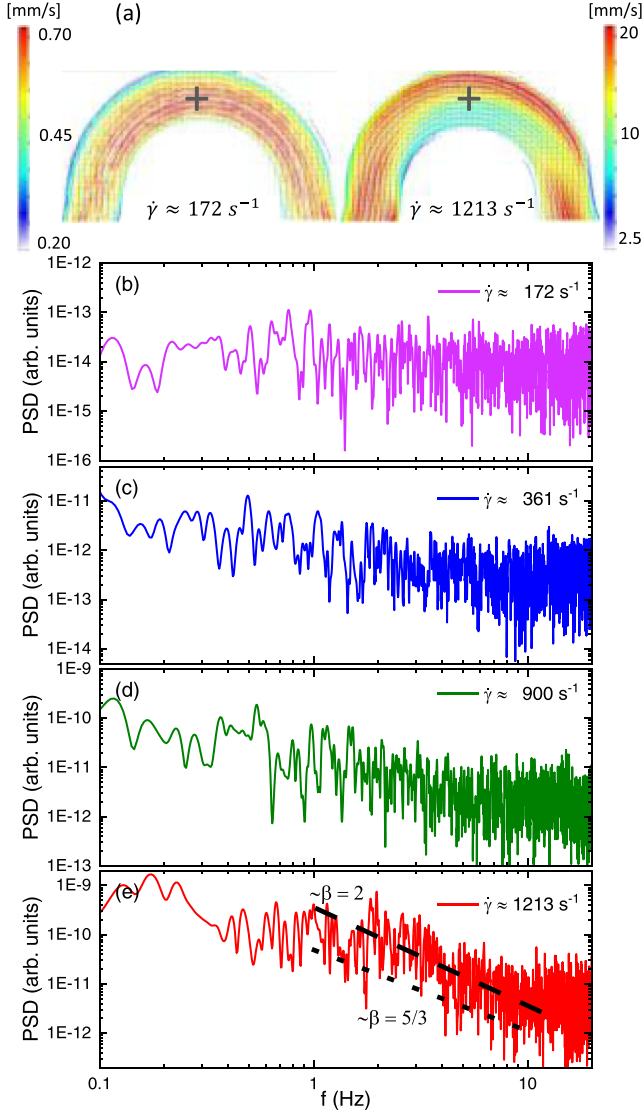
FIG. 2. (a) Time averaged velocity and streamlines obtained from $\mu$PIV for 0.200 wt% Flopaam 3630. [(b)–(e)] PSD analysis of velocity fluctuations at the center of serpentine channel indicated by a (+) sign in panel (a) for 0.200 wt% Flopaam 3630 at various shear rates below and above the critical shear rate. The dashed line indicates an exponential scaling with $\beta = 2$, and the dotted line represents the Kolmogorov scaling ($\beta = 5/3$) for comparison.

$\eta_0$ and $\eta_\infty$ are the zero-shear viscosity and viscosity at infinite shear rates, $\Lambda$ is a characteristic time, $n$ is the power law exponent associated with the degree of shear thinning, and $a$ is a transition control factor. In Eq. (2), the ratio of the shear-dependent viscosity $\eta(\dot{\gamma})$ to the shear modulus $G_0$ is equivalent to the relaxation time $\lambda(\dot{\gamma})$ [41,42]. The shear modulus $G_0$ is taken as the largest shear mode obtained from the generalized Maxwell model fitted to the small amplitude frequency sweep test results (data in the Supplemental Material [28]). This is a reasonable approximation of the shear modulus at relatively fast flows, corresponding to the range of shear rate at which purely elastic instability is observed in our experiments. To this end, $G(\omega) = G'(\omega) + iG''(\omega)$ is fitted to the frequency sweep test results with the least number of

relaxation elements required for a proper fit (typically $N = 4$), where $G'(\omega)$ and $G''(\omega)$ are given by Eqs. (4) and (5):

$$G'(\omega) = \sum_{k=1}^{N} G_k \frac{(\lambda_k \cdot \omega)^2}{1 + (\lambda_k \cdot \omega)^2}, \qquad (4)$$

$$G''(\omega) = \sum_{k=1}^{N} G_k \frac{\lambda_k \cdot \omega}{1 + (\lambda_k \cdot \omega)^2}. \qquad (5)$$

Shear modulus $G$ in general describes the elastic component of a viscoelastic material under shear in the viscoelastic fluid model, and is defined as $G = \tau/\gamma_e$, where $\gamma_e$ is the deformation of the elastic component.

In the following, we adapt the scaling of the nonlinear instability of the polymer solutions in the semidilute regime according to the White-Metzner fluid model. Since the relaxation time is shear dependent in the semidilute regime, the characteristic length nonlinearly increases with $\dot{\gamma}$ and is approximated by $l(\dot{\gamma}) = \lambda(\dot{\gamma})U = (\eta(\dot{\gamma})U)/G_0$. Streamlines of polymer flow in the serpentine channel obtained from $\mu$PIV generally follow the geometrical curvature of the channel [Fig. 2(a)]. Therefore, the minimum radius of the curved streamlines $\mathcal{R}$ in our experiments is approximated by the inner radius of the serpentine $r_i$. Thus, within the framework of the White-Metzner model, the threshold of the critical stress factor $M_{crit}$ at the onset of purely elastic instability in Eq. (1) is approximated by

$$\sqrt{\frac{\eta(\dot{\gamma})U}{G_0 \mathcal{R}} \frac{N_1(\dot{\gamma})}{2\eta(\dot{\gamma})\dot{\gamma}}} \geqslant M_{crit}. \qquad (6)$$

The average velocity in the serpentine channel is expressed as $U = Q/(WH)$. Since we consider the shear rate $\dot{\gamma}$ to depend linearly on the flow rate $Q$ and $\eta(\dot{\gamma})$ is canceled out, we approximate the critical stress factor $M_{crit}$ by Eq. (7). As previously mentioned, according to our point-wise approach, we obtain the relevant rheological properties of the polymer solution corresponding to the apparent shear rate $\dot{\gamma}_{crit}$ at onset of purely elastic instability:

$$C\sqrt{\frac{N_1(\dot{\gamma}_{crit})}{G_0}} \approx M_{crit}. \qquad (7)$$

Here, $C$ is a geometry constant computed as $C = (WH)/(64\pi \mathcal{R}^2)$ for a serpentine channel with rectangular cross section. Equation (7) suggests that, for a given geometry, $M_{crit}$ correlates solely with the ratio between the first normal stress difference at the onset of purely elastic instability, $N_1(\dot{\gamma}_{crit})$, and the shear modulus $G_0$ corresponding to the smallest relaxation mode. As explained earlier, the first normal stress difference is responsible for destabilizing the polymer flow in a curved geometry. On the other hand, the capacity of polymers to deform, i.e., their degree of elasticity is characterized by the value of the shear modulus. Therefore, the ratio of $N_1$ to $G_0$ is expected to be the decisive factor for the onset of instability.

Higher normalized concentration of a polymer solution correlates to higher degree of elasticity, and thus higher value of $G_0$. This means that the onset of purely elastic instability at higher normalized concentrations requires a larger $N_1$. Applying Eq. (7), we estimate $M_{crit}$ for our experiments as

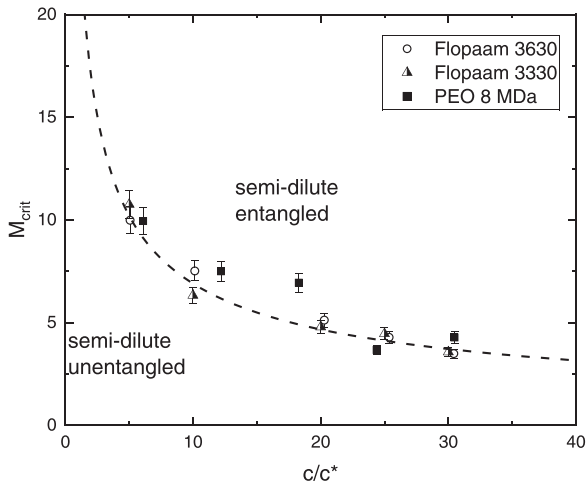FIG. 3. Threshold value $M_{crit}$ calculated from Eq. (7) as function of $c/c^\star$ for all utilized polymer solutions. The dashed curve is a power-law fit $M_{crit} = A \, (c/c^*)^{-b}$, where $A = (25.28 \pm 3.87)$ and $b = (0.56 \pm 0.05)$.

summarized in Table I and plotted in Fig. 3 as function of the normalized concentration $c/c^*$ for all polymer solutions used in this work. In fact, the estimated values for $M_{crit}$ collapse into a single master curve following a power law with an exponent of about $-0.56$. Qualitatively, this trend can be understood in view of the rheological differences observed in frequency sweep test between polymers below and above the entanglement concentration $10 \times c^*$. For unentangled polymer solutions, i.e., at $c/c^* < 10$ the loss modulus $G''(\omega)$ is always larger than the storage modulus $G'(\omega)$ for the entire range of frequencies [28]. This suggests that despite a significant elastic component in the fluid, viscous behavior

during flow is likely to dominate in this concentration regime, resulting in retardation of purely elastic instability. This means that purely elastic instability for $c/c^* < 10$ occurs at relatively higher shear rates, and thus $M_{crit}$ is relatively larger. The above argument is consistent with the discussion of Morozov *et al.*, who suggest that the Pakdel and McKinley criterion should be considered as a suitable asymptotic rule that is accurate only at sufficiently large degree of elasticity [4]. Indeed, for concentrations $c/c^* > 10$, i.e., in the semidilute entangled regime where the elastic component is entirely dominant, $M_{crit}$ approaches an asymptotic value of approximately 3.7.

In summary, we have studied the flow of semidilute polymer solutions in a geometrically well-defined serpentine channel and detected the occurrence of purely elastic instability via pressure measurement and $\mu$PIV. We have adapted the traditional scaling of the onset of purely elastic instability for polymer solutions in the semidilute regime by respecting the shear dependency of their rheological properties. As a consequence, our approach provides a realistic representation of the actual polymer behavior with respect to the flow by taking the rheological properties at the onset of instability into account. This, indeed, leads to a universal scaling as function of normalized concentration depending only on the ratio between the first normal stress difference $N_1(\dot{\gamma}_{crit})$ and the shear modulus $G_0$ regardless of the type of the polymer. As demonstrated, this scaling allows quantitative prediction of the onset of purely elastic instability for a wide range of high molecular weight polymer solutions.

[1] E. S. Shaqfeh, Annu. Rev. Fluid Mech. **28**, 129 (1996).

[2] A. Groisman and V. Steinberg, Nature (London) **405**, 53 (2000).

[3] T. Burghelea, E. Segre, and V. Steinberg, Phys. Rev. Lett. **96**, 214502 (2006).

[4] A. N. Morozov and W. van Saarloos, Phys. Rep. **447**, 112 (2007).

[5] V. Steinberg, Annu. Rev. Fluid Mech. **53**, 27 (2021).

[6] S. S. Datta, A. M. Ardekani, P. E. Arratia, A. N. Beris, I. Bischofberger, J. G. Eggers, J. E. López-Aguilar, S. M. Fielding, A. Frishman, M. D. Graham, J. S. Guasto, S. J. Haward, S. Hormozi, G. H. McKinley, R. J. Poole, A. Morozov, V. Shankar, E. S. G. Shaqfeh, A. Q. Shen, H. Stark *et al.*, arXiv:2108.09841.

[7] W. M. Abed, R. D. Whalley, D. J. Dennis, and R. J. Poole, J. Non-Newtonian Fluid Mech. **231**, 68 (2016).

[8] A. Groisman and V. Steinberg, Nature (London) **410**, 905 (2001).

[9] P. Shakeri, M. Jung, and R. Seemann, Phys. Fluids **33**, 113102 (2021).

[10] R. H. Ewoldt, M. T. Johnston, and L. M. Caretta, in *Complex Fluids in Biological Systems*, edited by S. Spagnolie, Biological

and Medical Physics, Biomedical Engineering (Springer, New York, NY, 2015), pp. 207–241.

[11] K. Hyun, M. Wilhelm, C. O. Klein, K. S. Cho, J. G. Nam, K. H. Ahn, S. J. Lee, R. H. Ewoldt, and G. H. McKinley, Prog. Polym. Sci. **36**, 1697 (2011).

[12] B. Meulenbroek, C. Storm, V. Bertola, C. Wagner, D. Bonn, and W. van Saarloos, Phys. Rev. Lett. **90**, 024502 (2003).

[13] P. Pakdel and G. H. McKinley, Phys. Rev. Lett. **77**, 2459 (1996).

[14] G. H. McKinley, P. Pakdel, and A. Öztekin, J. Non-Newtonian Fluid Mech. **67**, 19 (1996).

[15] S. J. Haward, G. H. McKinley, and A. Q. Shen, Sci. Rep. **6**, 33029 (2016).

[16] G. Yao, J. Zhao, H. Yang, M. A. Haruna, and D. Wen, Phys. Fluids **31**, 123106 (2019).

[17] A. Groisman and V. Steinberg, New J. Phys. **6**, 29 (2004).

[18] J. Zilz, R. J. Poole, M. A. Alves, D. Bartolo, B. Levaché, and A. Lindner, J. Fluid Mech. **712**, 203 (2012).

[19] A. Souliès, J. Aubril, C. Castelain, and T. Burghelea, Phys. Fluids **29**, 083102 (2017).

[20] L. Pan, A. Morozov, C. Wagner, and P. E. Arratia, Phys. Rev. Lett. **110**, 174502 (2013).

[21] R. B. Bird, C. F. Curtiss, R. C. Armstrong, and O. Hassager, *Dynamics of Polymeric Liquids*, 2nd ed., Kinetic Theory, Vol. 2 (Wiley-Interscience, New York, 1987).

[22] T. Burghelea and V. Bertola, *Transport Phenomena in Complex Fluids*, CISM International Centre for Mechanical Sciences (Springer, Cham, 2020), Vol. 598.

[23] Y. Jun and V. Steinberg, Phys. Rev. Lett. **102**, 124503 (2009).

[24] Y. Liu, Y. Jun, and V. Steinberg, J. Rheol. **53**, 1069 (2009).

[25] L. Casanellas, M. A. Alves, R. J. Poole, S. Lerouge, and A. Lindner, Soft Matter **12**, 6167 (2016).

[26] M. Jung, M. Brinkmann, R. Seemann, T. Hiller, M. Sanchez de La Lama, and S. Herminghaus, Phys. Rev. Fluids **1**, 074202 (2016).

[27] A. V. Dobrynin, R. H. Colby, and M. Rubinstein, Macromolecules **28**, 1859 (1995).

[28] See Supplemental Material at http://link.aps.org/supplemental/ 10.1103/PhysRevE.105.L052501 for rheological characterisation of the utilized polymer solutions and additional information to the $\mu$PIV measurements.

[29] T. G. Mezger, *The Rheology Handbook: For Users of Rotational and Oscillatory Rheometers* (Vincentz Network, Hannover, 2006).

[30] A. M. Howe, A. Clarke, and D. Giernalczyk, Soft Matter **11**, 6419 (2015).

[31] D. Rivero, L. M. Gouveia, A. J. Müller, and A. E. Sáez, Rheol. Acta **51**, 13 (2012).

[32] O. Arnolds, H. Buggisch, D. Sachsenheimer, and N. Willenbacher, Rheol. Acta **49**, 1207 (2010).

[33] A. Machado, H. Bodiguel, J. Beaumont, G. Clisson, and A. Colin, Biomicrofluidics **10**, 043507 (2016).

[34] Y. Son, Polymer **48**, 632 (2007).

[35] J. P. Hartnett and M. Kostic, in *Advances in Heat Transfer* (Academic Press, New York, 1989), Vol. 19, pp. 247–356.

[36] A. Collyer and D. Clegg, *Rheological Measurements* (Springer, Berlin, 1998).

[37] A. N. Kolmogorov, Proc. R. Soc. London, Ser. A **434**, 15 (1991).

[38] J. Beaumont, H. Bodiguel, and A. Colin, Soft Matter **9**, 10174 (2013).

[39] D. Kawale, E. Marques, P. L. Zitha, M. T. Kreutzer, W. R. Rossen, and P. E. Boukany, Soft Matter **13**, 765 (2017).

[40] H. Bodiguel, J. Beaumont, A. Machado, L. Martinie, H. Kellay, and A. Colin, Phys. Rev. Lett. **114**, 028302 (2015).

[41] J. L. White and A. B. Metzner, J. Appl. Polym. Sci. **7**, 1867 (1963).

[42] H.-C. Tseng, Phys. Fluids **33**, 057115 (2021).